

Article

Net Electron Capture in Collisions of Multiply Charged Projectiles with Biologically Relevant Molecules

Hans Jürgen Lüdde ^{1,*}, Alba Jorge ^{2,*}, Marko Horbatsch ^{2,*} and Tom Kirchner ^{3,*}¹ Center for Scientific Computing, Goethe-Universität, D-60438 Frankfurt, Germany² Departamento de Química, Universidad Autónoma de Madrid, 28049 Madrid, Spain³ Department of Physics and Astronomy, York University, Toronto, ON M3J 1P3, Canada

* Correspondence: luedde@itp.uni-frankfurt.de (H.J.L.); alba.jorge@uam.es (A.J.); marko@yorku.ca (M.H.); tomk@yorku.ca (T.K.)

† These authors contributed equally to this work.

Received: 27 July 2020; Accepted: 15 September 2020; Published: 17 September 2020



Abstract: A model for the description of proton collisions from molecules composed of atoms such as hydrogen, carbon, nitrogen, oxygen and phosphorus (H, C, N, O, P) was recently extended to treat collisions with multiply charged ions with a focus on net ionization. Here we complement the work by focusing on net capture. The ion–atom collisions are computed using the two-center basis generator method. The atomic net capture cross sections are then used to assemble two models for ion–molecule collisions: An independent atom model (IAM) based on the Bragg additivity rule (labeled IAM-AR), and also the so-called pixel-counting method (IAM-PCM) which introduces dependence on the orientation of the molecule during impact. The IAM-PCM leads to significantly reduced capture cross sections relative to IAM-AR at low energies, since it takes into account the overlap of effective atomic cross sectional areas. We compare our results with available experimental and other theoretical data focusing on water vapor (H₂O), methane (CH₄) and uracil (C₄H₄N₂O₂). For the water molecule target we also provide results from a classical-trajectory Monte Carlo approach that includes dynamical screening effects on projectile and target. For small molecules dominated by a many-electron atom, such as carbon in methane or oxygen in water, we find a saturation phenomenon for higher projectile charges ($q = 3$) and low energies, where the net capture cross section for the molecule is dominated by the net cross section for the many-electron atom, and the net capture cross section is not proportional to the total number of valence electrons.

Keywords: ion–atom collisions; ion–molecule collisions; capture processes; computational methods

1. Introduction

Collisions of multiply charged ions with biologically relevant molecules are recognized as being important for future developments in radiation medicine and related fields. The importance of measuring and theoretically analyzing ionization, as well as electron capture, has been stressed in many works. Reviews concerning the application of heavy-ion beams in tumor therapy can be found in References [1,2]. Two types of investigation are needed when considering ion–molecule collisions in this context: On the one hand one needs to understand the fundamental process, i.e., scattering outcomes under single-collision conditions which can be compared to experiments at this level (vapor or gas-phase targets); on the other hand one needs Monte-Carlo simulations of how the energy deposition process occurs. The present work falls into the first category. It deals with electron capture by multiply charged ions. The detailed understanding of capture processes is needed for simulations of energy deposition for multiple reasons: first of all, they contribute considerably to

recoil ion and fragment production; second, they lead to neutralized projectiles also contributing to energy deposition.

There are numerous experimental efforts which focus largely on differential electron emission, but integrated ionization, electron capture, and excitation cross sections are also relevant since they contribute to energy deposition, and stopping power. A recent example is the study of net ionization in $C^{6+} - CH_4$ collisions [3]. When we refer to net capture and net ionization, respectively, we remind the reader that these are weighted summed cross sections with the electron multiplicity appearing as a weight. For ionization this corresponds to the total number of electrons observed in the continuum, and for capture it corresponds to the total amount of charge transferred to the projectile. Some authors refer to these as total cross sections. We mostly avoid this term due to its ambiguity (in general, the term total cross section is used for integrated versus differential cross section, and also total ionization, or total capture in some works refers to the summed cross sections without weighting by the multiplicity). In some limits, e.g., ionization at very high energies for multiply charged projectiles single-electron processes may dominate and the difference between net and total (non-weighted summed) cross sections for ionization or capture becomes small or even negligible. Another comment worth making in this context is that net capture includes transfer ionization processes (simultaneous capture and ionization), and likewise net ionization includes these processes, as well. The net cross sections are also referred to as gross cross sections in the literature to distinguish them from total or summed cross sections, cf. Ref [4].

On the theoretical side one finds several methods that attempt to explain the experimental data. Often provided alongside with the experimental work is the continuum distorted wave with eikonal initial state (CDW-EIS) method. Differential electron emission can be obtained also directly from a classical-trajectory Monte Carlo (CTMC) method, which for water molecule targets was enhanced recently to include dynamical screening effects [5]. The CTMC approach takes the (frozen) molecular orientation into account during the collision, and total ionization cross sections, as well as some charge-state correlated cross sections have been compared to experimental data [6].

Another approach is to use collision information obtained for the atomic constituents and to combine them into molecular cross sections, most notably independent atom models (IAM), which either follow the simple Bragg additivity rule (labeled IAM-AR), or more sophisticated versions that take the molecular structure of the target into account, and allow for the fact that the effective cross section should be reduced due to overlap effects. The latter, named pixel counting method (labeled IAM-PCM), tested originally for proton impact [7–10] was used recently to investigate scaling behavior of net ionization as a function of projectile charge [11].

The CDW-EIS work also relies on ion–atom collision calculations, and includes some molecular effects on the basis of a Mulliken population analysis. For the ionization problem we found that CDW-EIS and CTMC calculations with frozen potentials generally are close to IAM-AR results, while the CTMC calculations with dynamical screening [6] are closer to IAM-PCM absolute cross sections [11], which are lower in the vicinity of the ionization maximum and merge with IAM-AR results only at very high energies when the projectile charge is high, i.e., $q > 1$. The reduction in ionization cross sections (whether in the IAM-PCM results versus IAM-AR or CTMC with versus without dynamical screening) can easily reach a factor of two.

In the present paper we focus on an analogous problem at lower collision energies, namely the net capture problem. Here the ion–atom cross sections grow quickly with projectile charge, and the overlap and orientation problem again becomes important for the molecular targets. The experimental situation is more scarce in the case of capture as compared to ionization, and therefore theoretical support is even more important.

The paper is organized as follows. In Section 2 we introduce the theoretical basis for the current work. Section 2.1 presents new results for two-center basis generator method (TC-BGM) ion–atom calculations for He^{2+} and Li^{3+} projectiles; for atomic hydrogen targets the results are compared with theory and experiment. In Section 2.2 we provide a summary of the IAM-PCM methodology and

briefly describe the CTMC time-dependent mean field approach which is applied to the water molecule target. Section 3 serves to provide a detailed comparison with experimental data and a selection of other theoretical work; in Section 3.1 we present results for water, where we also compare with CTMC results with and without dynamical screening; in Section 3.2 we present results for methane for which we demonstrate a saturation effect in the case of projectile charges $q = 3$, and Section 3.3 contains results for uracil. The paper ends with a few concluding remarks in Section 4. Atomic units, characterized by $\hbar = m_e = e = 4\pi\epsilon_0 = 1$, are used unless otherwise stated.

2. Model

2.1. Ion–Atom Collisions

The independent atom models rely on state-of-the-art ion–atom collision calculations. In Figure 1 we show the results of the two-center basis generator method (TC-BGM) calculations for atomic targets that form the constituents of biologically relevant molecules (hydrogen, carbon, nitrogen, oxygen, and phosphorus). Experimental verification is only available for atomic hydrogen, as is theoretical confirmation by other state-of-the-art methods, namely the convergent close coupling (CCC) approach [12,13], and a two-center atomic orbital expansion method based on Gaussian-type orbitals [14].

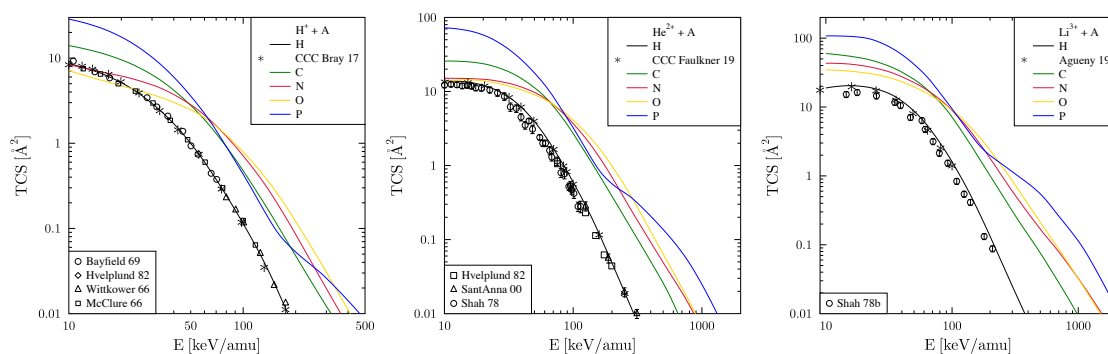


Figure 1. In the left panel the net capture cross sections for protons colliding with atoms H, C, N, O, P is shown (solid lines) as calculated with the two-center basis generator method (TC-BGM) using basis sets described in the text, the middle panel is for He^{2+} projectiles, while the right panel is for the case of Li^{3+} projectiles. For atomic hydrogen targets and proton and He^{2+} projectiles the results are compared with the convergent close coupling calculation of References [12,13], respectively. For Li^{3+} impact we compare with data from Reference [14]. For proton impact the experimental data are from References [15–18], for He^{2+} impact from References [18–20], and for $\text{Li}^{3+} - \text{H}$ collisions from Reference [21].

The present TC-BGM ion–atom calculations are as described in Reference [11]: For proton impact a projectile potential W_P hierarchy is obtained on the basis of explicitly including shells up to principal quantum number $n_P = n_T = 4$ on projectile and target, respectively, for $q = 2$ projectiles we used $n_P = 6$ and $n_T = 5$, while for $q = 3$ the explicitly included basis was expanded to $n_P = 7$ and $n_T = 5$. These explicitly included states are complemented by states that represent the continuum using the TC-BGM approach [8,22].

For the many-electron atoms the theoretical modelling is at the level of exchange-only density functional theory using the optimized potential method. Therefore, electron correlation effects are not included in these calculations [23,24].

The results for proton and He^{2+} impact on atomic hydrogen display excellent agreement with experiments and with CCC theory over several orders of magnitude. For projectile charge $q = 3$, i.e., Li^{3+} projectiles, our results are slightly higher than the experimental data, but are in very good agreement with the recently reported calculations of Reference [14]. Not shown in Figure 1 for proton and He^{2+} impact are the calculations of Reference [14]. They agree very well the TC-BGM and CCC results for protons and are slightly lower (at the 10% level for energies 25–100 keV/amu) for He^{2+} projectiles.

The structure of these cross sections is simple. Notable is the increase in net capture as one reduces the collision energy towards 10 keV/amu, with cross section values short of 8 \AA^2 for protons, 12 \AA^2 for $q = 2$, and a value of 20 \AA^2 reached already at 30 keV/amu for bare lithium projectiles.

For the atoms containing more than one electron capture from the outer shells becomes large even for intermediate energies with patterns that are not totally straightforward when one compares $q = 1, 2, 3$. Capture from phosphorus reaches 100 \AA^2 for $q = 3$ at low energies, and electron capture from carbon atoms is also very strong. This provides a background for interesting effects when combining these cross sections to make predictions for molecular targets.

For phosphorus atoms there are notable structures in the capture cross sections at higher energies which are related to shell effects. For collision energies below 200 keV/amu capture from the M-shell dominates, but at higher energies capture from the L-shell becomes more important. This was investigated, e.g., in Reference [22] for p–Na collisions.

2.2. Ion–Molecule Collisions

The present work reports on calculations of several theoretical models. On the one hand we compare two independent atom models: (i) In the naive case, namely the additivity rule based model (IAM-AR), the atomic capture cross sections described in Section 2.1 are simply added together and completely ignore molecular structure; (ii) in the more sophisticated pixel counting method (IAM-PCM) molecular structure is introduced by a geometric procedure, which will be briefly reviewed below. For the water molecule target we also report results from two classical-trajectory models.

The IAM-PCM has been described and illustrated in detail in previous papers, most notably References [7,10]. Reference [10] highlights the role played by the contributions from the time evolution of occupied orbitals from different atomic species to the net cross sections. The model is compared there to a methodology employed by the community that uses the CDW-EIS approach, which also uses ion–atom calculations, and incorporates molecular eigenenergies on the basis of quantum molecular structure calculations while employing complete neglect of differential overlap (CNDO), i.e., a Mulliken population analysis [25,26].

In essence the IAM-PCM approach is based on an interpretation of the atomic net cross sections as geometrical areas, e.g., areas that correspond to the net capture (or net ionization) cross section. Rather than summing up all these areas (as assumed by the additivity rule, i.e., the IAM-AR) a pixel counting method is used to measure the effective cross-sectional area that emerges when one eliminates overlaps between cross sections from different atoms encountered by the projectile. Therefore, the effective molecular cross sectional area is defined as a function of molecular orientation. The latter is chosen randomly, and is sampled to obtain converged cross sections. A critical discussion of the merits of this procedure (potential emphasis on atoms encountered first) is found in Reference [8], where it is argued that for net cross sections the method should certainly be appropriate. An illustration of the method is given below in Section 3.2 where we observe a saturation behavior of the cross section for $q \geq 3$ projectiles colliding with methane (CH_4).

For a detailed description of the other method for which we show results for water molecule vapor targets, namely the CTMC model, we also refer to previous literature. Calculations with frozen target potential on the basis of a three-center potential are reported in References [27,28]. This effective potential, used in the classical statistical ensemble simulation, is drawing information from quantum structure calculations. It yields accepted values for the orbital energies, and in addition to CTMC calculations, it was also used for numerical grid solutions of the time-dependent Schrödinger equation [29]. An extension of this model which can be considered a semiclassical ($\hbar = 0$) approximation to the quantum problem is presented in Reference [5] where the potential parameters were allowed to vary dynamically as a function of the average (net) ionization state of the water molecule. This resulted in a substantial reduction of the net ionization cross section (by up to a factor of two) compared to the static potential model results. A further extension was carried out recently where the projectile potential was also allowed to be varied as a function of the average (net) charge state of the projectile [6].

Both the static-potential CTMC and the dynamically screened model are sensitive to the orientation of the molecule during the collision. Therefore, the comparison with IAM-PCM and IAM-AR calculations is of great interest. Concerning capture data there is one problem that needs to be addressed in the CTMC approach: For high energies capture from inner shells in target atoms (or molecules) becomes problematic in a classical-trajectory model, because it becomes possible to capture into orbits well below the allowed 1s-level, i.e., orbits with binding energies larger than $q^2/2$ begin to occur. These classically allowed capture contributions need to be removed from the analysis. For proton impact ($q = 1$) this correction becomes significant at impact energies of 200 keV/amu and higher, for $q > 1$ this point moves to higher energies. The correction procedure is based on a prescription to associate principal quantum numbers n_P with energy ranges [30].

3. Comparison with Experiments

3.1. Collisions with Water Vapor (H_2O)

In Figure 2 we compare the theoretical model results for proton impact on water vapor with experiment. We note that the IAM-PCM results are corrected compared to those shown in References [7,8] (the wrong bond length was applied in those calculations), and they agree now well within error bars at low energies with the experimental data of Rudd et al. [31]. The IAM-AR results (which are independent of the molecular structure and remain unchanged) overestimate the low-energy experimental data by up to a factor of two.

The two CTMC model calculations are expected to yield very similar results, since dynamical screening on the projectile is not turned on for $q = 1$, and dynamical screening on the target is expected to be small. At medium to low energies both CTMC model calculations fall in between the IAM-PCM and IAM-AR results and are consistent with experiment (at the upper end of their errors). The inset which uses a semilogarithmic presentation shows that the model with dynamical screening is close to IAM-PCM, and still consistent with the experimental data of Reference [31].

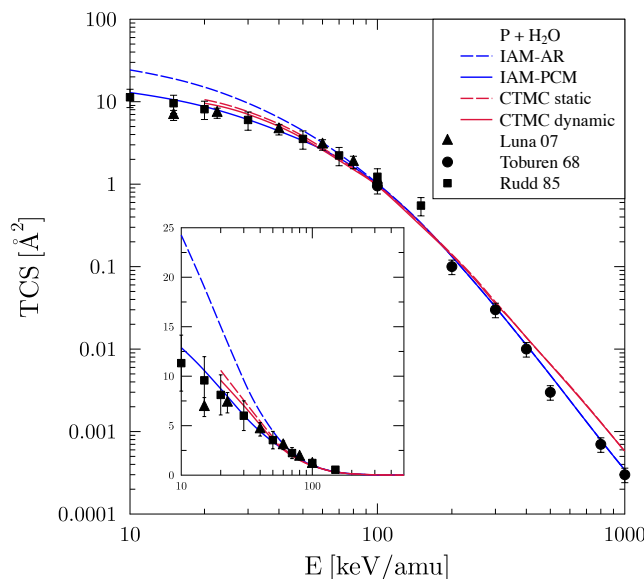


Figure 2. Net electron capture cross section for proton-water collisions. The highest curve (dashed blue) shows the Bragg additivity rule result (IAM-AR), the lowest (solid blue) curve the IAM-PCM result. In between are the classical-trajectory Monte Carlo (CTMC) results, namely the (dashed red) static-potential CTMC, and below it (solid red) the dynamical-screening CTMC result. The experimental data are from References [31–33].

In Figure 3 we present our results for He^{2+} impact on water vapor. The IAM-PCM results follow the trend of the experimental data of Reference [34] very well, particularly at the lowest energies shown. The IAM-AR model overestimates them by a factor of two at the lowest energies. The CTMC calculations with static potential are close to the IAM-AR results at intermediate and high energies. The CTMC time-dependent mean-field model calculation, on the other hand, is closer to the IAM-PCM results and overestimates them by about 20–30% at low to medium energies. For higher energies all models are practically in agreement. The experimental data are obtained by summing single and double-capture contributions ($\sigma_{\text{net}} = \sigma_1 + 2\sigma_2$), which have error estimates of 12% and 16% respectively.

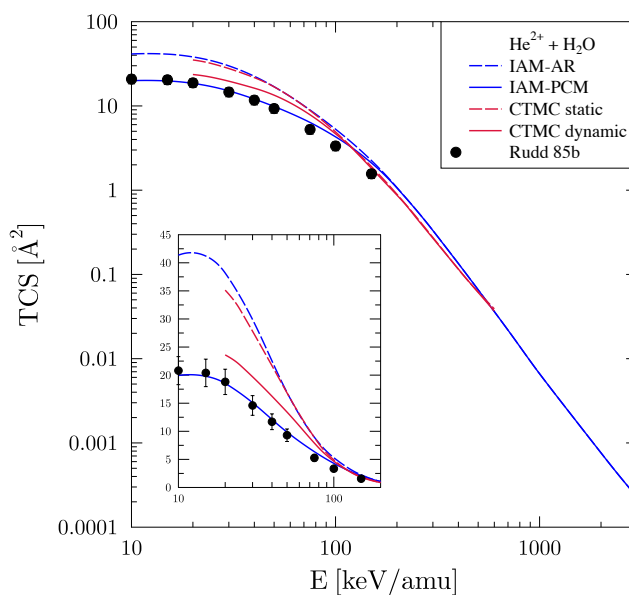


Figure 3. Net electron capture cross section for He^{2+} -water collisions. The curves follow the same pattern as described for Figure 2. The experimental data are from Reference [34].

For Li^{3+} -water vapor collisions the trend observed for He^{2+} impact continues as shown in Figure 4: The calculated net capture cross sections continue to grow with projectile charge q , and the gap between IAM-PCM and IAM-AR remains at a factor-of-two increase for the naive Bragg-additivity-rule-based model. The static-potential CTMC calculations side with this IAM-AR result, while the CTMC time-dependent mean-field calculation is again only 20–30% above the IAM-PCM result at low to medium energies.

At energies above 200 keV/amu the models merge and agree well with the experimental data of Reference [35]. The two data points below this energy are below all calculated values, reaching a factor-of-two discrepancy at 100 keV/amu. This shortfall of the experimental data goes hand-in-hand with an observed shortfall in double-ionization contributions in this energy range as compared to TC-BGM calculations for pure ionization (cf. Figure 7 of Reference [35]) and transfer ionization (cf. Figure 8 of Reference [35]). Note that these transfer ionization channels contribute both to net capture and net ionization. This shortfall in ionized electron flux in the experimental data is difficult to understand in the context of modelling the projectile charge state dependence both in the IAM-PCM [11] and the time-dependent mean-field CTMC model [6], and thus we can only ask for additional experimental work in this context.

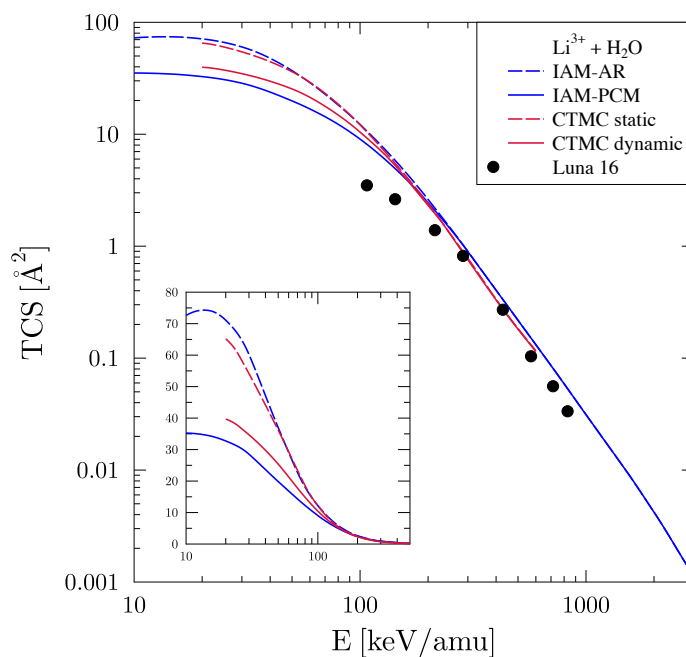


Figure 4. Net electron capture cross section for Li^{3+} -water collisions. The curves follow the same pattern as described for Figure 2. The experimental data are from Reference [35].

3.2. Collisions with Methane (CH_4)

IAM-PCM and IAM-AR results for net capture of electrons from methane by proton impact were described previously in Reference [10], where they were compared with other theoretical works, namely CDW-EIS and CNDO calculations. The CDW-EIS method was applied to higher projectile charges in Reference [26].

In Figure 5 we compare the net capture cross sections from IAM-AR and IAM-PCM for projectile charges $q = 1, 2, 3$. For the methane target the difference between the two models at the lowest energy reported exceeds a factor of two. For He^{2+} impact the experimental data fall below the present IAM-PCM results, and merge with the proton impact data at 10 keV/amu collision energy.

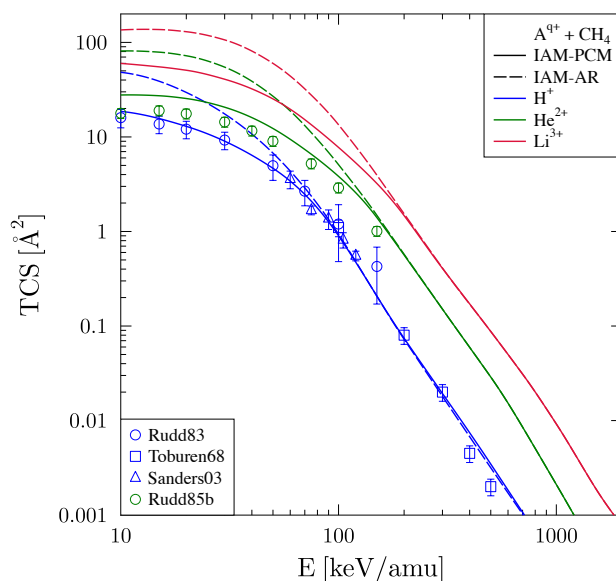


Figure 5. Net electron capture cross section for collisions of protons, He^{2+} , and Li^{3+} ions with methane (CH_4). The dashed curves show the IAM-AR results, while the solid curves are obtained with the IAM-PCM. The curves merge at lower energies for proton impact (shown in blue), followed by He^{2+} impact (shown in green), and even higher energies for Li^{3+} projectiles (shown in red). The experimental data are from References [32,34,36,37].

For Li^{3+} projectiles we find that the net capture cross section at low energies becomes 60 \AA^2 , which is the same value that is reached by $\text{Li}^{3+} - \text{C}$ collisions (cf. Figure 1). This can be called a saturation behavior in the sense that it is not the total number of valence electrons that determines the size of net cross sections for high projectile charges. We first investigate this phenomenon in detail for methane, and then make some comments further below as to which other target molecules will be affected in a similar way. Looking at the equivalent comparison of $\text{Li}^{3+} - \text{H}_2\text{O}$ (Figure 4) vs. $\text{Li}^{3+} - \text{O}$ (Figure 1) collisions, we observe the same effect with a common value of about 35 \AA^2 .

The saturation behavior in the net capture cross section as one goes to low impact energies and higher projectile charges can be illustrated as an overlap effect in the IAM-PCM. A geometric condition for the saturation behavior in CH_4 is obtained from the following consideration: if r_C and r_H are the radii of the carbon and hydrogen cross-sectional disks with $r_X = \sqrt{\sigma_X/\pi}$ and b the bond length of C-H, then saturation happens if $r_C \geq r_H + b$. For molecules which involve large bond lengths saturation is much less likely to occur.

As shown in Figure 1 net electron capture from carbon atoms for low energies exceeds net capture from atomic hydrogen by more than a factor of two for $q = 3$ projectiles. The saturation condition $r_C \geq r_H + b$ is fulfilled up to $E \approx 80 \text{ keV/amu}$. As a result of saturation the IAM-PCM cross section becomes independent of the orientation of the methane molecule. This overlap effect is demonstrated for methane in Figure 6 and analogous figures can be drawn for water vapor.

To further illustrate the saturation phenomenon we show in Figure 7 a direct comparison between the IAM-PCM net capture cross sections for ion-methane collisions with those for the same process involving carbon atoms. With increasing projectile charge q the two cross sections merge. This feature would be a strong test for the IAM-PCM if experimental capture cross sections for ion-carbon collisions were available.

Clearly, saturation in the sense that the cross section of just one atom becomes an effective bound for the molecular cross section is not achievable for large molecules. If, however, saturation does occur (as was found in methane for carbon atoms vs. hydrogen) then one can generalize, namely one finds $\sigma_{\text{CH}_4} = \sigma_C = \sigma_{\text{CH}_3} = \sigma_{\text{CH}_2}$, i.e., the cross sections of the functional groups CH_3 and CH_2 are also limited by the cross section of carbon. For pure hydrocarbons (alkanes, alkenes, alkynes,

aromatics, etc.) this means that within the IAM-PCM they can be described as carbon clusters with molecular geometry.

A similar situation concerning saturation is found for other functional groups of biorelevant molecules. For example, the cross section for the hydroxyl group (OH) is restricted by the atomic cross section of O, just like the amino group (NH₂) by N and phosphate (PO₄) is limited by the cross section of P. This simplifies the treatment of large biomolecules considerably in the case of saturation, as they can be approximated by an IAM-PCM model of the dominant atoms (C, N, O, P) at the molecular positions of their respective functional groups.

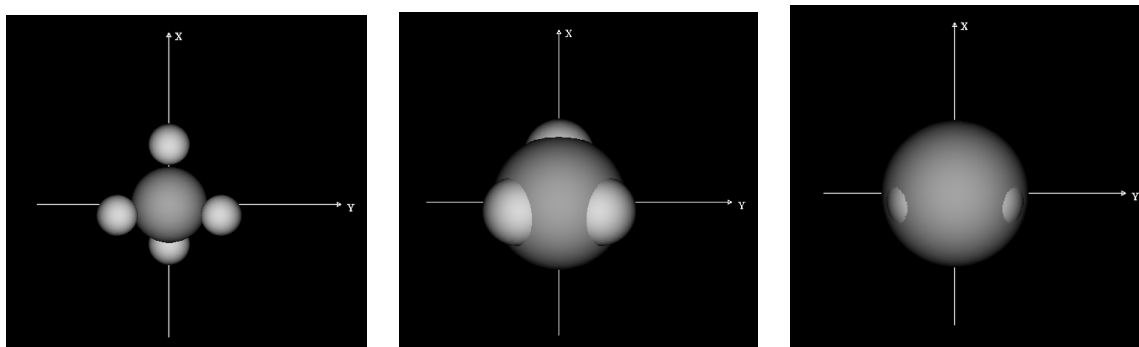


Figure 6. Demonstration of the overlap effect in IAM-PCM: For a particular orientation the effective net capture cross section is obtained from overlapping the atomic cross sections for the carbon atom and the four hydrogens at a collision energy of 70 keV/amu. Left panel for proton impact ($q = 1$), middle panel for He²⁺ ($q = 2$), and right panel for $q = 3$.

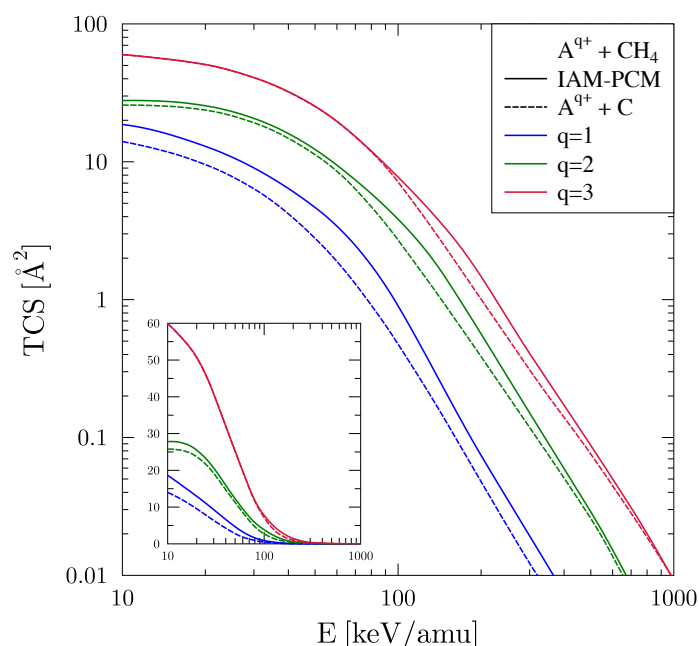


Figure 7. Net electron capture cross sections as functions of impact energy for collisions of protons, He²⁺, and Li³⁺ ions with methane (CH₄) calculated in the IAM-PCM are compared to net capture from carbon atoms (short dashed lines) as calculated by the TC-BGM (cf. red curves in Figure 1). The top curve pair (in red) is for Li³⁺ projectiles, the middle curve pair (in green) for He²⁺ projectiles and the bottom pair (in blue) for proton impact.

3.3. Collisions with Uracil ($C_4H_4N_2O_2$)

For large biologically relevant molecules the saturation phenomenon will occur at another level, namely the combinations of large contributor atoms (e.g., multiples of carbon, nitrogen) may again lead to a reduction of the cross sections due to overlap. While it may seem that the hydrogen atoms are ‘covered’ up by the overlap effect for high projectile charges and low collision energies, they do, of course, contribute to the capture process, particularly if there are multiples of them. One should keep in mind that net capture includes transfer ionization processes, i.e., for $q = 3$ net capture involves more than three electrons. The overlap of net cross sections, i.e., of the geometric areas is naturally dominated by atoms which on account of their valence shells can make big contributions of their own. The uracil molecule is an interesting candidate to look into the phenomenon.

We begin with a comparison of the net capture cross sections for our three projectiles with charges $q = 1, 2, 3$ in Figure 8. The structure of the cross sections as a function of collision energy is similar to that obtained for methane (cf. Figure 5), although the magnitude of the cross sections is substantially larger due to the increased number of valence electrons. This is particularly the case for the Bragg additivity rule based result (IAM-AR), and less so for IAM-PCM. For Li^{3+} projectiles at the lowest energies shown this cross section for uracil is larger compared to that for methane by a factor of 1.5. This is in contrast with the IAM-AR results, where this factor is about four. We are not aware of experimental data for these cross sections with $q > 1$, and therefore we cannot verify this aspect of the IAM-PCM prediction.

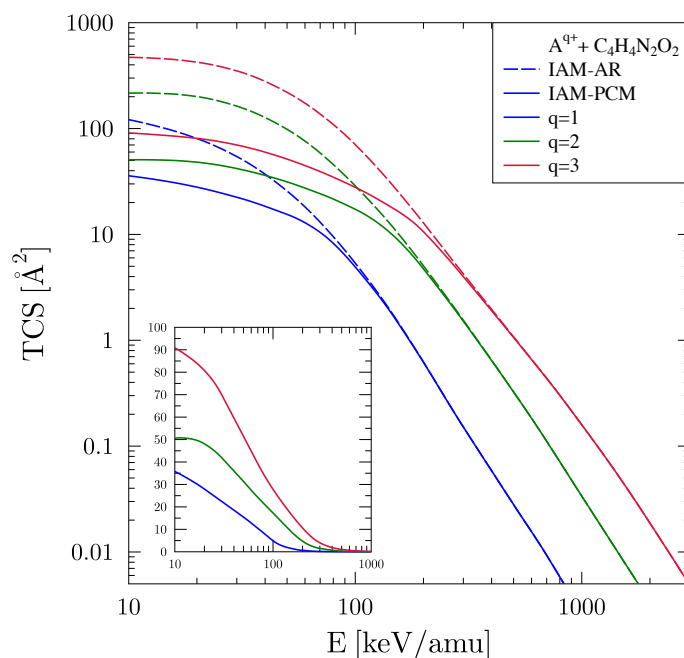


Figure 8. Net electron capture cross section for collisions of protons, He^{2+} , and Li^{3+} ions with uracil ($C_4H_4N_2O_2$). The dashed curves show the IAM-AR results, while the solid curves are obtained with the IAM-PCM. The curves merge at lower energies for proton impact (shown in blue), followed by He^{2+} impact (shown in green), and even higher energies for Li^{3+} projectiles (shown in red).

In Figure 9 we compare our present results with the experimental data and with other theoretical data for proton impact. The experimental data of Tabet et al. [38] are higher than all theories shown for the energy range 40–150 keV. At energies above 100 keV where both our IAM calculations merge they fall in-between the CDW and CDW-EIS results of Champion et al. [39]. The distorted-wave CNDO calculations of Purkait et al. [40,41] cross the CDW results, while being lower below 100 keV and higher above the transition point in energy where the IAM-AR and IAM-PCM results merge. At low energies the IAM-PCM results are clearly the lowest by about a factor of three.

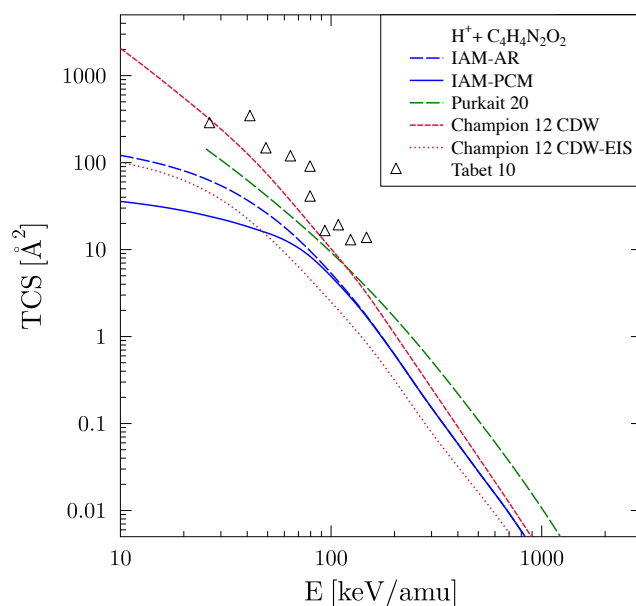


Figure 9. Net electron capture cross section for collisions of protons with uracil ($C_4H_4N_2O_2$). The blue dashed curves show the IAM-AR results, while the blue solid curves are obtained with the IAM-PCM. The experimental data are from Reference [38], the other theoretical data are from References [39–41]. A lower bound for the experimental uncertainties (not shown) can be estimated from the electron capture branching ratio (shown in Figure 1 of Reference [38]) to be on the order of 20% at the lowest energy and a few percent at the highest energies. For a detailed discussion of estimated experimental errors we refer to Reference [42].

4. Conclusions

As a follow-up to our previous work on net ionization of biologically relevant molecules by highly charged ions [11] we have presented results for net capture for three molecules. The choice of water and methane was motivated by the existence of some experimental data, while uracil is an example of a substantially larger molecule. Comparison with other theories shows that a number of them yield cross sections that are in the vicinity of Bragg additivity rule results (IAM-AR). For all molecules considered the IAM-PCM yields significantly reduced net capture cross sections at low energies with a particularly strong effect for higher projectile charges.

For the water molecule two classical trajectory based simulations were used, the standard CTMC model was generally found to be closer to the IAM-AR results, while the recently introduced time-dependent mean-field CTMC model at least partially supports the decrease in net capture cross sections provided by the IAM-PCM.

The IAM-PCM predicts that the net capture cross sections will saturate for high projectile charge by the presence of large contributions from constituent atoms with large valence electron number. For small molecules the effect was demonstrated (CH_4 cross sections are dominated by net cross sections from C, and likewise for H_2O vs. O targets), while for uracil the cross sections are dominated by the leading atoms (C, N, O). Future work may involve an investigation as to why many of the larger biomolecules have such similar cross sections, based on the notion that the dominant atoms (C, N, O, P) located at their positions will control the net cross sections through their effective geometric scattering cross sectional areas.

Author Contributions: H.J.L., A.J., M.H. and T.K. have contributed equally to this work. All authors have read and agreed to the published version of the manuscript.

Funding: This research was funded by the Natural Sciences and Engineering Research Council of Canada (NSERC) under grants RGPIN-2017-05655 and RGPIN-2019-06305.

Acknowledgments: We would like to thank the Center for Scientific Computing, University of Frankfurt for making their High Performance Computing facilities available.

Conflicts of Interest: The authors declare no conflict of interest.

Abbreviations

The following abbreviations are used in this manuscript:

IAM-AR	Independent atom model—additivity rule
IAM-PCM	Independent atom model—pixel counting method
CDW-EIS	Continuum distorted wave with eikonal initial state
CTMC	Classical trajectory Monte Carlo
TC-BGM	Two-center basis generator method
CCC	Convergent close coupling
CNDO	Complete neglect of differential overlap

References

1. Schardt, D.; Elsässer, T.; Schulz-Ertner, D. Heavy-ion tumor therapy: Physical and radiobiological benefits. *Rev. Mod. Phys.* **2010**, *82*, 383–425. [[CrossRef](#)]
2. Nikjoo, H.; Emfietzoglou, D.; Liamsuwan, T.; Taleei, R.; Liljequist, D.; Uehara, S. Radiation track, DNA damage and response—A review. *Rep. Prog. Phys.* **2016**, *79*, 116601. [[CrossRef](#)]
3. Mandal, A.; Bagdia, C.; Roy Chowdhury, M.; Bhattacharjee, S.; Misra, D.; Monti, J.M.; Rivarola, R.D.; Tribedi, L.C. Electron emission from CH₄ molecules in collisions with fast bare C ions. *Phys. Rev. A* **2020**, *101*, 062708. [[CrossRef](#)]
4. Montanari, C.C.; Miraglia, J.E. Antiproton, proton and electron impact multiple ionization of rare gases. *J. Phys. B At. Mol. Opt. Phys.* **2012**, *45*, 105201. [[CrossRef](#)]
5. Jorge, A.; Horbatsch, M.; Illescas, C.; Kirchner, T. Classical-trajectory Monte Carlo calculations of differential electron-emission cross sections in fast heavy-ion collisions with water molecules. *Phys. Rev. A* **2019**, *99*, 062701. [[CrossRef](#)]
6. Jorge, A.; Horbatsch, M.; Kirchner, T. Multicharged-ion–water-molecule collisions in a classical-trajectory time-dependent mean-field theory. *Phys. Rev. A* **2020**, *102*, 012808. [[CrossRef](#)]
7. Lüdde, H.J.; Achenbach, A.; Kalkbrenner, T.; Jankowiak, H.C.; Kirchner, T. An independent-atom-model description of ion–molecule collisions including geometric screening corrections. *Eur. Phys. J. D* **2016**, *70*, 82. [[CrossRef](#)]
8. Lüdde, H.J.; Horbatsch, M.; Kirchner, T. A screened independent atom model for the description of ion collisions from atomic and molecular clusters. *Eur. Phys. J. B* **2018**, *91*, 99. [[CrossRef](#)]
9. Lüdde, H.J.; Horbatsch, M.; Kirchner, T. Proton-impact-induced electron emission from biologically relevant molecules studied with a screened independent atom model. *J. Phys. B* **2019**, *52*, 195203. [[CrossRef](#)]
10. Lüdde, H.J.; Horbatsch, M.; Kirchner, T. Electron capture and ionization cross-section calculations for proton collisions with methane and the DNA and RNA nucleobases. *Eur. Phys. J. D* **2019**, *73*, 249. [[CrossRef](#)]
11. Lüdde, H.J.; Kalkbrenner, T.; Horbatsch, M.; Kirchner, T. Nonperturbative scaling behavior for net ionization of biologically relevant molecules by multiply charged heavy-ion impact. *Phys. Rev. A* **2020**, *101*, 062709. [[CrossRef](#)]
12. Bray, I.; Abdurakhmanov, I.B.; Bailey, J.J.; Bray, A.W.; Fursa, D.V.; Kadyrov, A.S.; Rawlins, C.M.; Savage, J.S.; Stelbovics, A.T.; Zammit, M.C. Convergent close-coupling approach to light and heavy projectile scattering on atomic and molecular hydrogen. *J. Phys. B At. Mol. Opt. Phys.* **2017**, *50*, 202001. [[CrossRef](#)]
13. Faulkner, J.; Abdurakhmanov, I.B.; Alladustov, S.U.; Kadyrov, A.S.; Bray, I. Electron capture, excitation and ionization in He²⁺-H and H⁺-He⁺ collisions. *Plasma Phys. Control. Fusion* **2019**, *61*, 095005. [[CrossRef](#)]
14. Agueny, H.; Hansen, J.P.; Dubois, A.; Makhoute, A.; Taoutioui, A.; Sisourat, N. Electron capture, ionization and excitation cross sections for keV collisions between fully stripped ions and atomic hydrogen in ground and excited states. *At. Data Nucl. Data Tables* **2019**, *129–130*, 101281. [[CrossRef](#)]
15. McClure, G.W. Electron Transfer in Proton-Hydrogen-Atom Collisions: 2–117 keV. *Phys. Rev.* **1966**, *148*, 47–54. [[CrossRef](#)]

16. Bayfield, J.E. Measurement of the Total Cross Section for Charge Transfer into the Metastable State H(2s) for Proton Collisions with Atomic Hydrogen. *Phys. Rev.* **1969**, *185*, 105–112. [[CrossRef](#)]
17. Wittkower, A.B.; Ryding, G.; Gilbody, H.B. An experimental study of charge transfer in proton-atomic-hydrogen collisions using a furnace target method. *Proc. Phys. Soc.* **1966**, *89*, 541–546. [[CrossRef](#)]
18. Hvelplund, P.; Andersen, A. Electron Capture by Fast H⁺, He⁺, and He²⁺ Ions in Collisions With Atomic and Molecular Hydrogen. *Phys. Scr.* **1982**, *26*, 375–380. [[CrossRef](#)]
19. Shah, M.B.; Gilbody, H.B. Electron capture and He⁺(2s) formation in fast He²⁺-H and He⁺-H collisions. *J. Phys. B At. Mol. Phys.* **1978**, *11*, 121–131. [[CrossRef](#)]
20. Sant’Anna, M.M.; Melo, W.S.; Santos, A.C.F.; de Jesus, V.L.B.; Shah, M.B.; Sigaud, G.M.; Montenegro, E.C.; Busnengo, H.F.; Corchs, S.E.; Rivarola, R.D.; et al. Electronic capture by He²⁺ from atomic and molecular hydrogen. *Phys. Rev. A* **2000**, *61*, 052717. [[CrossRef](#)]
21. Shah, M.B.; Goffe, T.V.; Gilbody, H.B. Electron capture and loss by fast lithium ions in H and H₂. *J. Phys. B At. Mol. Phys.* **1978**, *11*, L233–L236. [[CrossRef](#)]
22. Zapukhlyak, M.; Kirchner, T.; Lüdde, H.J.; Knoop, S.; Morgenstern, R.; Hoekstra, R. Inner- and outer-shell electron dynamics in proton collisions with sodium atoms. *J. Phys. B* **2005**, *38*, 2353. [[CrossRef](#)]
23. Engel, E.; Vosko, S.H. Accurate optimized-potential-model solutions for spherical spin-polarized atoms: Evidence for limitations of the exchange-only local spin-density and generalized-gradient approximations. *Phys. Rev. A* **1993**, *47*, 2800–2811. [[CrossRef](#)] [[PubMed](#)]
24. Talman, J.D.; Shadwick, W.F. Optimized effective atomic central potential. *Phys. Rev. A* **1976**, *14*, 36–40. [[CrossRef](#)]
25. Galassi, M.E.; Rivarola, R.D.; Beuve, M.; Olivera, G.H.; Fainstein, P.D. Theoretical calculation of single ionization in collisions between protons and low-Z molecules at intermediate and high energies. *Phys. Rev. A* **2000**, *62*, 022701. [[CrossRef](#)]
26. Quinto, M.A.; Montenegro, P.R.; Monti, J.M.; Fojón, O.A.; Rivarola, R.D. Electron capture by swift ions from molecules of biological interest. *J. Phys. B At. Mol. Opt. Phys.* **2018**, *51*, 165201. [[CrossRef](#)]
27. Illescas, C.; Errea, L.F.; Méndez, L.; Pons, B.; Rabadán, I.; Riera, A. Classical treatment of ion-H₂O collisions with a three-center model potential. *Phys. Rev. A* **2011**, *83*, 052704. [[CrossRef](#)]
28. Illescas, C.; Lombana, M.A.; Méndez, L.; Rabadán, I.; Suárez, J. Ionization and electron capture in Li³⁺ + H₂O collisions. *J. Phys. Conf. Ser.* **2020**, *1412*, 162006. [[CrossRef](#)]
29. Errea, L.; Illescas, C.; Méndez, L.; Rabadán, I.; Suárez, J. Lattice description of electron loss in high-energy H⁺+H₂O collisions. *Chem. Phys.* **2015**, *462*, 17–22. [[CrossRef](#)]
30. Becker, R.L.; MacKellar, A.D. Theoretical initial *l* dependence of ion-Rydberg-atom collision cross sections. *J. Phys. B At. Mol. Phys.* **1984**, *17*, 3923–3942. [[CrossRef](#)]
31. Rudd, M.E.; Goffe, T.V.; DuBois, R.D.; Toburen, L.H. Cross sections for ionization of water vapor by 7–4000-keV protons. *Phys. Rev. A* **1985**, *31*, 492–494. [[CrossRef](#)] [[PubMed](#)]
32. Toburen, L.H.; Nakai, M.Y.; Langley, R.A. Measurement of High-Energy Charge-Transfer Cross Sections for Incident Protons and Atomic Hydrogen in Various Gases. *Phys. Rev.* **1968**, *171*, 114–122. [[CrossRef](#)]
33. Luna, H.; de Barros, A.L.F.; Wyer, J.A.; Scully, S.W.J.; Lecointre, J.; Garcia, P.M.Y.; Sigaud, G.M.; Santos, A.C.F.; Senthil, V.; Shah, M.B.; et al. Water-molecule dissociation by proton and hydrogen impact. *Phys. Rev. A* **2007**, *75*, 042711. [[CrossRef](#)]
34. Rudd, M.E.; Goffe, T.V.; Itoh, A. Ionization cross sections for 10–300-keV/u and electron-capture cross sections for 5–150-keV/u ³He²⁺ ions in gases. *Phys. Rev. A* **1985**, *32*, 2128–2133. [[CrossRef](#)]
35. Luna, H.; Wolff, W.; Montenegro, E.C.; Tavares, A.C.; Lüdde, H.J.; Schenk, G.; Horbatsch, M.; Kirchner, T. Ionization and electron-capture cross sections for single- and multiple-electron removal from H₂O by Li³⁺ impact. *Phys. Rev. A* **2016**, *93*, 052705. [[CrossRef](#)]
36. Rudd, M.E.; DuBois, R.D.; Toburen, L.H.; Ratcliffe, C.A.; Goffe, T.V. Cross sections for ionization of gases by 5-4000-keV protons and for electron capture by 5-150-keV protons. *Phys. Rev. A* **1983**, *28*, 3244–3257. [[CrossRef](#)]
37. Sanders, J.M.; Varghese, S.L.; Fleming, C.H.; Soosai, G.A. Electron capture by protons and electron loss from hydrogen atoms in collisions with hydrocarbon and hydrogen molecules in the 60–120 keV energy range. *J. Phys. B At. Mol. Opt. Phys.* **2003**, *36*, 3835–3846. [[CrossRef](#)]

38. Tabet, J.; Eden, S.; Feil, S.; Abdoul-Carime, H.; Farizon, B.; Farizon, M.; Ouaskit, S.; Märk, T.D. 20–150-keV proton-impact-induced ionization of uracil: Fragmentation ratios and branching ratios for electron capture and direct ionization. *Phys. Rev. A* **2010**, *81*, 012711. [[CrossRef](#)]
39. Champion, C.; Weck, P.F.; Lekadir, H.; Galassi, M.E.; Fojón, O.A.; Abufager, P.; Rivarola, R.D.; Hanssen, J. Proton-induced single electron capture on DNA/RNA bases. *Phys. Med. Biol.* **2012**, *57*, 3039–3049. [[CrossRef](#)]
40. Sammadar, S.; Purkait, K.; Halder, S.; Mondal, A.; Mandal, C.; Purkait, M. Electron-capture process induced by bare ion impact on biological targets. *J. Energy Power Eng.* **2019**, *13*, 413–26. [[CrossRef](#)]
41. Purkait, K.; Purkait, M. Cross sections for electron capture process of biological molecules by proton and α -particle impact. *J. Phys. Conf. Ser.* **2020**, *1412*, 162009. [[CrossRef](#)]
42. Tabet, J.; Eden, S.; Feil, S.; Abdoul-Carime, H.; Farizon, B.; Farizon, M.; Ouaskit, S.; Märk, T.D. Absolute total and partial cross sections for ionization of nucleobases by proton impact in the Bragg peak velocity range. *Phys. Rev. A* **2010**, *82*, 022703. [[CrossRef](#)]



© 2020 by the authors. Licensee MDPI, Basel, Switzerland. This article is an open access article distributed under the terms and conditions of the Creative Commons Attribution (CC BY) license (<http://creativecommons.org/licenses/by/4.0/>).